Combining Germanium Quantum Dots with Porous Silicon: An Innovative Method for X-ray Detection

AHMAD M. AL-DIABAT[1,*], NATHEER A. ALGADRI[2], TARIQ ALZOUBI[3], NASER M. AHMED[4], ABDULSALAM ABUELSAMEN[5], OSAMA ABU NOQTA[6], GHASEB N. MAKHADMEH[5,7], AMAL MOHAMED AHMED ALI[8], ALMUTERY AML[9]

[1]Department of Physics, Al-Zaytoonah University of Jordan,
Amman,
JORDAN

[2]Department of Physics,
Isra University, Amman,
JORDAN

[3]College of Engineering and Technology, American University of the Middle East,
Egaila, 54200,
KUWAIT

[4]School of Physics, Universiti Sains Malaysia,
Penang,
MALAYSIA

[5]Medical Imaging and Radiography Department, Aqaba University of Technology, Aqaba 910122,
JORDAN

[6]MEU Research Unit, Middle East University,
Amman 11831,
JORDAN

[7]General Education Department, Skyline University College,
Sharjah, P. O. Box 1797,
UAE

[8]Prince Sattam Bin Abdulaziz University,
Alkharj 11942,
SAUDI ARABIA

[9]Department of Physics, Shaqra University,
SAUDI ARABIA

**Corresponding Author*

Abstract: - This study investigates the controlled electrochemical synthesis of porous silicon and germanium (Ge)-doped porous silicon using a 4:1 ratio of hydrofluoric acid (HF) to ethanol. Structural analysis performed with FESEM-EDX confirmed the presence of Ge in the samples. Analysis of the I-V characteristics demonstrated that increasing the bias voltage at the source led to a corresponding increase in the observed current. Additionally, effective X-ray measurements facilitated the assessment of X-ray irradiation effects on the sample detector. The experimental results indicated that the optimal conditions for the porous silicon (PS) and Ge-doped porous silicon (Ge-PS) samples were (90V, 100mA, 1s) and (100V, 10mA, 0.5s), respectively.

Key-Words: - porous silicon, X-ray detector, Quantum dots, EGFET, Ge/PS, Radiation.

Received: April 19, 2024. Revised: October 23, 2024. Accepted: November 7, 2024. Published: December 10, 2024.

1 Introduction

Radiation refers to the emission and transfer of energy in the form of electromagnetic waves (EM waves) or particles, such as electrons and neutrons, traveling through space or various materials. It is primarily categorized into two types: ionizing and non-ionizing radiation. Ionizing radiation possesses sufficient energy to ionize atoms by ejecting electrons from their orbitals, which occurs when energy is transferred through waves or particles. Examples of ionizing radiation include X-rays, gamma rays, and neutrons, while non-ionizing radiation, such as radio and microwave frequencies, lacks the energy needed for ionization, [1], [2].

X-ray detectors operate by leveraging the photoelectric conversion capabilities of semiconductors to transform X-rays into electrical signals. Directly ionizing radiation comprises highly charged particles that quickly transfer energy through interactions with orbital electrons. In contrast, indirectly ionizing radiation, like X-rays or gamma rays, interacts with atoms, resulting in electron ejection and energy deposition within the material, [3].

X-ray detectors are widely utilized in various domains, including industrial inspection, scientific research, non-destructive testing, and medical imaging, [4], [5], [6]. Solid-state semiconductor detectors are particularly favored for their simplicity, compactness, durability, and versatility in creating detector arrays for imaging applications. They convert X-ray photons into electrical signals rapidly, and key performance metrics—such as efficiency, sensitivity, and peak-to-background ratio—are crucial for minimizing patient X-ray exposure and enhancing the detection of faint X-ray signals, [7], [8] [9] [10]. These performance metrics correlate with properties such as charge carrier mobility, lifetime product, and the atomic number (Z) of the semiconductor material. A range of materials, primarily crystalline, such as silicon, germanium, and cadmium zinc telluride, are utilized in X-ray detector fabrication, benefiting from advancements in semiconductor technology. With ongoing technological progress, researchers are increasingly investigating nanoparticles and exploring diverse synthesis methods to produce either crystalline or amorphous nanomaterials tailored for specific applications. Common synthesis techniques include chemical vapor deposition (CVD), reduction of graphene oxide, and chemical exfoliation, particularly for materials like graphene and carbon nanotubes (CNTs), [11], [12].

Quantum dots, a specific type of nanoparticle composed of a limited number of atoms, facilitate electron transfer. Woggon has extensively studied their optical properties, particularly their light absorption capabilities. When excited by ultraviolet (UV) light, a quantum dot semiconductor emits light at a specific wavelength, producing a unique color, [13]. The electronic, magnetic, and optical characteristics of quantum dots can be significantly influenced by variations in their shape and size, especially when doped with other materials.

Porous silicon (PS), characterized by its silicon composition with voids, was first discovered at Bell Laboratories in the mid-1950s by Uhlir during research on electrochemical machining techniques for silicon wafers in microelectronics. Contrary to expectations, the wafers did not dissolve uniformly, resulting in the formation of voids in the <100> orientation. Although initially overlooked, this material regained interest in the 1980s due to its high surface area, which proved beneficial for spectroscopic applications, [14], [15].

Doping PS with Ge quantum dots was chosen to potentially enhance its detection capabilities. The additional electrons from Ge improve the material's sensitivity to low-level irradiation, [16]. Research on this specific doping method for irradiation applications is limited, prompting I-V characteristic measurements to be taken post-synthesis to assess the impact of irradiation on the detector.

Two primary dosimeter types in the semiconductor industry are silicon diodes and Metal Oxide In the semiconductor industry, the two main types of dosimeters are silicon diodes and Metal Oxide Semiconductor Field Effect Transistors (MOSFETs). However, the extended gate field effect transistor (EGFET) offers advantages such as a smaller size, which facilitates fabrication and handling, making it suitable for various applications, [17]. It also provides low-sensitivity detection with high accuracy in irradiation measurements. Continued exploration of material properties may result in enhanced efficiency for radiation detectors. Each type of dosimeter presents distinct advantages and limitations in radiation detection. Semiconductor detectors generally exhibit a more pronounced response compared to ionization chamber detectors. Therefore, this study primarily focuses on semiconductor-based detectors, [16].

This research aims to investigate the integration of germanium quantum dots with porous silicon and evaluate their effectiveness as X-ray detectors. The study will concentrate on fabrication methods, the material properties of the resulting composite, and the performance of the detection device. Ultimately, the goal is to demonstrate how combining these two materials can advance X-ray detection technology, potentially leading to significant improvements in this field.

2 Methodology

Electrochemical etching is used to prepare PS because it is inexpensive and produces a sufficient quantity. The preparation procedure is separated into four stages: cutting, cleaning, electrochemical, and washing. Initially, a silicon wafer is sliced into a square form of 2 x 2 cm using an ATV RV-129 diamond scriber machine. After that, the standard Radio Corporation of America (RCA) cleaned the sliced samples. Werner Kern created the RCA technique at the RCA Laboratory in the late 1960s. It includes the following chemical processes: organic and particle cleaning (RCA-1), oxide stripping, and ionic cleaning (RCA-2). After cleaning the surface impurities from the wafer, its weight is carefully measured and recorded. The wafer is then secured at the base of a Teflon cell, ensuring contact with a metal plate. To initiate the electrochemical process, a mixed electrolyte solution containing hydrofluoric acid (HF) and ethanol (C_2H_5OH, 99.99%) in a 4:1 volume ratio is introduced into the Teflon cell. For Ge deposition on PS, 0.05g of Ge powder is combined with a 4:1 combination of HF and ethanol. After Ge is dissolved in the solution, the electrochemical process begins with 20 mA current and a 20-minute etching duration. After 20 minutes, the solution is discarded as trash, and the PS is repeatedly cleaned with ethanol. The weight of the sample following the etching process is measured and documented.

A Field Emission Scanning Electron Microscope (FESEM) is used to investigate the morphology, metallographic features, and topology of a material. It is a sophisticated approach for investigating materials' local structure (2-5nm), particle and grain form or size, and nanoscale element analysis, [18]. Thus, this approach is appropriate for viewing structures as small as 1nm on the material's surface. This experiment measures, records, analyzes, and discusses the properties of the I-V curve.

This study contrasts the presence and absence of light on the sample detector, using a tungsten lamp as a light source. After acquiring and analyzing the data from the I-V curves, the setup was modified somewhat, with the sample converted into a single electrode and put under an X-ray source to detect photons. As part of this investigation, the sample detector is converted into an EGFET (Extended Gate Field Effect Transistor). This experiment is designed to investigate radiation changes that occur on samples. Figure 1 depicts the experimental setup for an X-ray detector.

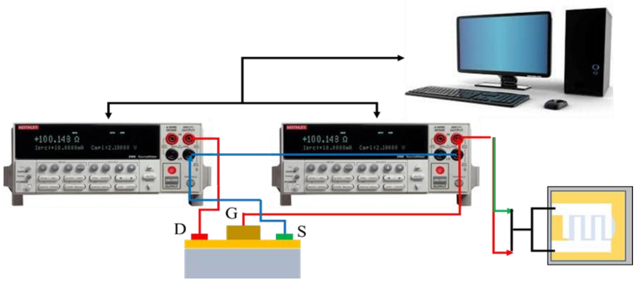

Fig. 1: Experimental setup for X-ray detector

3 Results And Discussion

3.1 Morphological Observations

Following the synthesis of all samples, FESEM/EDX was performed. The average pore size is determined. The average pore size for PS is around 420.88 nm. There are 'branches' on the surface of PS. Unlike PS, Ge-PS has more apparent pores. Chemical composition may be determined using FESEM and EDX, which are closely linked. Ge deposition was found in the samples. Because of the low mass of deposits utilized in the electrochemical process (0.05g of deposits in each sample), it is difficult to detect deposits on the sample's surface. All samples include impurities, including some polluted with boron (B), fluoride (F), and copper (Cu) particles.

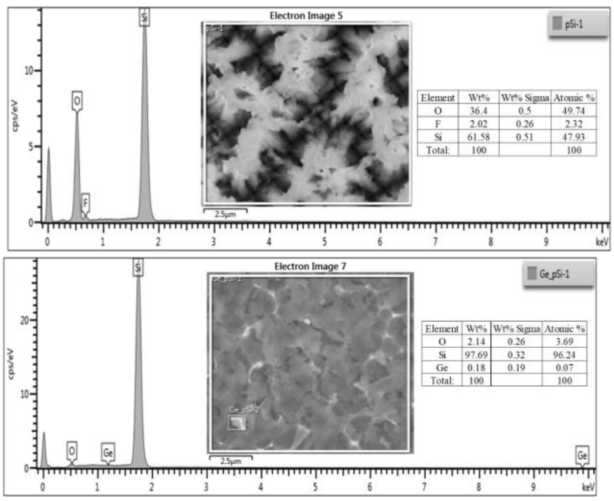

Element	Wt%	Wt% Sigma	Atomic %
O	36.4	0.5	49.74
F	2.02	0.26	2.32
Si	61.58	0.51	47.93
Total:	100		100

Element	Wt%	Wt% Sigma	Atomic %
O	2.14	0.26	3.69
Si	97.69	0.32	96.24
Ge	0.18	0.19	0.07
Total:	100		100

Fig. 2: FESEM/EDX result of (a) PS (b) Ge-PS

Figure 2 shows that porous silicon (PS) displays prominent peaks for silicon (Si) and oxygen (O), indicating a potential oxide layer formation on the sample surface. Furthermore, germanium (Ge) is detected in the Ge-PS sample with a concentration of 0.18% by weight (0.07% atomic.

3.2 I-V Characteristic Result

The I-V curve was recorded after the placement of interdigitated finger electrodes on the sample, as shown in Figure 3. This study primarily examined how light, specifically within the wavelength range of 380 to 700 nm, affects the sample detector's performance. A voltage was applied from the drain to the source, ranging from -5V to 5V, with the gate bias voltage set at either 0V or 0.3V.

The findings reveal that the gate bias voltage significantly influences detector performance across all samples. When the gate bias was raised to 0.3V, the current measured also increased. For instance, with a drain voltage of -5V, the current in PS at a 0V bias without light was approximately 2.0×10^{-5} A. However, with a gate bias of 0.3V, the current rose substantially to around 7.0×10^{-4} A.

This behavior can be attributed to the elevated gate bias voltage, which repels electrons from the gate surface, thereby allowing increased current flow through the drain. Thus, an increase in gate bias voltage correlates with a higher current flow. This observation is consistent with prior studies, which found that higher gate bias voltages result in increased current at a fixed drain voltage, [19].

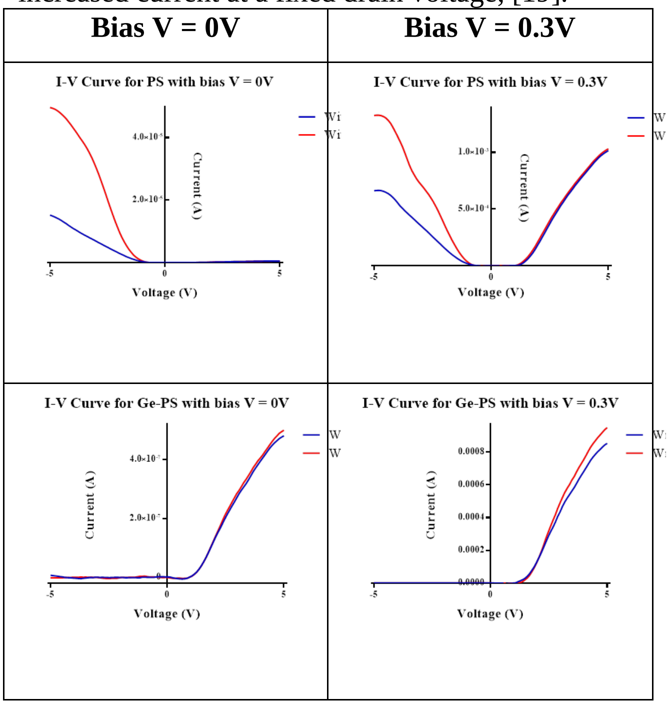

Fig. 3: I-V curve of PS, and Ge-PS at bias V = 0V & 0.3V

In this part of the study, it was observed that the current increases under the same applied voltage in the presence of light, with the exception of Ge-PS at a bias of 0.3V. The noticeable differences between the curves under light conditions indicate an enhanced recombination of electron-hole pairs. Studies show that when light photons interact with semiconductor materials, electrons in the valence band can absorb photon energy and transition to the conduction band, creating additional holes in the valence band. Figure 4 provides a schematic representation of the impact of light photons on the energy band gap.

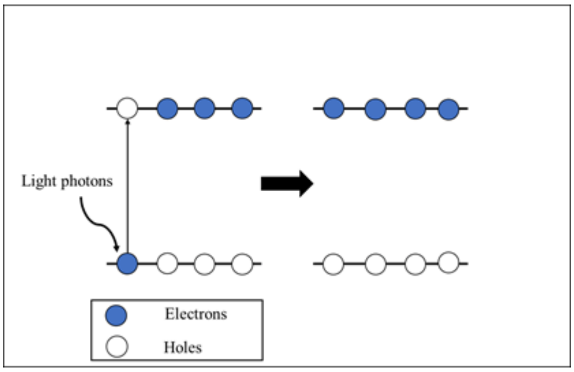

Fig. 4: Effects of light photons on energy band gap.

Here's a completed Table 1 summarizing the maximum and minimum current measurements for applied voltages of -5V and 5V at bias voltages of 0V and 0.3V.

Table 1. Maximum and minimum current measured for applied voltage (-5V and 5V) at bias 0V and 0.3 V

Sample	Bias 0V				Bias 0.3V			
	V=-5 V		V=5 V		V= -5 V		V=5 V	
Light	P	A	P	A	P	A	P	P
PS/I (A)	4.90×10^{-5}	1.60×10^{-5}	5.27×10^{-7}	4.99×10^{-7}	1.35×10^{-3}	6.23×10^{-4}	1.05×10^{-3}	1.04×10^{-3}
Ge-PS/I (A)	7.34×10^{-9}	8.73×10^{-9}	5.13×10^{-7}	4.85×10^{-7}	1.73×10^{-9}	4.74×10^{-9}	9.68×10^{-4}	8.70×10^{-4}

3.3 X-ray Detector Results

A detector sample underwent exposure to X-rays, followed by the collection of data for analysis. The study will evaluate and compare several parameters related to the X-ray exposure for each detector sample, with results presented in current versus time and voltage versus time graphs. This investigation seeks to examine and contrast the effects of varying irradiation conditions on the detector samples. The attributes of each detector will be assessed according to the parameters listed in Table 2.

Table 2. Parameters used for irradiated samples

Short name	Description
Without X-ray	Samples are not irradiated with X-ray/ normal condition.
(90, 100, 1)	Samples were irradiated at 90 V, 100mA, and 1s.
(100, 100, 1)	Samples were irradiated at 100 V, 100mA, and 1s.
(90, 100, 0.5)	Samples were irradiated at 90 V, 100mA, and 0.5s.

In a separate investigation known as the five-pulse study, a sample detector was subjected to five continuous irradiations under fixed X-ray parameters. This study aimed to collect pulse data displayed in current vs. time and voltage vs. time graphs, with the applied voltage maintained at 3 V for a duration of 5 seconds across the sample detectors.

As observed in the I-V characteristic study, increasing the gate bias voltage correlates with higher current detection, particularly notable at a bias of 0.5 V. In the current vs. time graphs, the irradiated sample took longer to achieve the same current levels compared to the non-irradiated sample. For example, in the current vs. time graph for porous silicon (PS) at a 0.3 V bias, the non-irradiated sample reached a current of 0.0002 A in 2.87 seconds, whereas the irradiated counterpart took 4.26 seconds (Figure 5 and Figure 6).

For non-irradiated samples, the applied voltage at 2 seconds was approximately 1 V for PS, after which the current began to rise from 0 A. In contrast, irradiated samples exhibited a slight delay in voltage response accompanied by a pulse, visible in both the voltage vs. time and current vs. time graphs, with the voltage graph displaying fluctuating pulses and the current graph showing smaller pulses.

Under the irradiation conditions of (90, 100, 1) and (100, 100, 1), a pulse was recorded at 0.45 seconds with a corresponding current of 12.7 μA. For the (90, 100, 0.5) condition, the pulse occurred at 2.82 seconds, yielding a measured current of 16.4 μA. In the voltage vs. time graph, the pulses for (90, 100, 1) and (100, 100, 1) were measured at 0.572 V and 0.465 V, respectively, after 2 seconds, while a pulse of 0.444 V was observed before 2 seconds for the (90, 100, 0.5) condition. Both current and voltage pulses were notably higher under a 0.5 V bias (Table 3).

Table 3. Current and voltage pulses measured for PS at bias 0.3V and 0.5V

Sample	Pulses measured		
	Parameters	Current vs time (μA)	Voltage vs time (V)
PS (bias 0.3V)	(90, 100, 1)	12.7	0.572
	(100, 100, 1)	12.7	0.465
	(90, 100, 0.5)	16.4	0.444
PS (bias 0.5V)	(90, 100, 1)	15.9	0.177, 0.775, 0.657
	(100, 100, 1)	26.6	0.956, 0.583
	(90, 100, 0.5)	26.6	0.7, 0.337

Graph of Current vs Time	Graph of Voltage vs Time

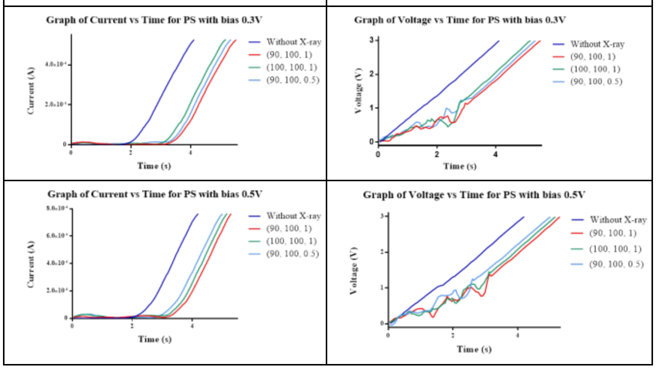

Fig. 5: Graph for PS with different parameters of X-ray irradiation

Graph of Current vs Time	Graph of Voltage vs Time

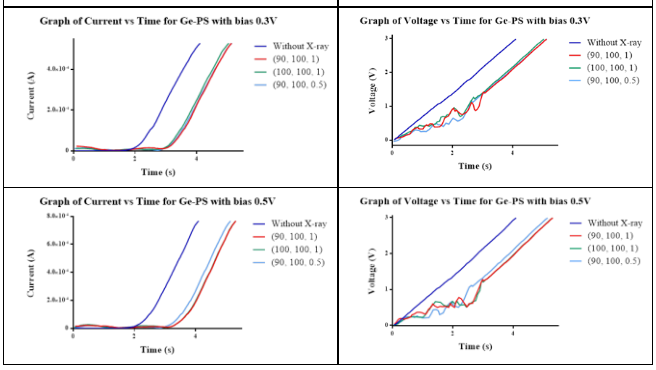

Fig. 6: Graph for Ge-PS with different X-ray parameters

The exploration of different parameters did not reveal significant variations in the samples' responses. Theoretically, X-ray irradiation is expected to cause a rapid surge in both voltage and current due to the extra energy it provides for electrons to move from the valence band to the conduction band. However, contrary to these expectations, the results showed a delay in the increases of voltage and current after irradiation, indicating that the data might be influenced by reverse bias voltage effects.

Additionally, the limited range of parameters used likely contributed to the minimal variation in pulse characteristics, restricting the observable differences. Consequently, this study primarily illustrates that the synthesized sample detector is indeed responsive to irradiation.

4 Conclusion

This study presents an innovative use of nanotechnology in radiation detection, highlighting the cost-effective production of extended gate field-effect transistors (EGFETs). The fabrication of PS and Ge/PS extended gates employed an electrochemical method utilizing a 4:1 HF/ethanol mixture along with 0.05 g of doping powder. The characterization through FESEM/EDX analysis confirmed the presence of the doping material, yielding distinct imaging results.

In contrast to other studies, the I-V characteristics were obtained using this unique approach. The investigation also included the impact of X-ray irradiation on the EGFET sample detector, with measurements and results thoroughly documented. Notably, the Ge-PS sample detector demonstrated a more significant difference in current and voltage pulses than the PS detector. Based on the findings, optimal parameters for each detector type are suggested: (90 V, 100 mA, 1 s) for PS and (100 V, 10 mA, 0.5 s) for Ge-PS.

Acknowledgement:
The authors acknowledge the financial support from Al Zaytoonah University of Jordan under grant number 2022-2021/08/16.

Declaration of Generative AI and AI-assisted Technologies in the Writing Process

During the preparation of this work the authors used AI servises in order to improve grammar and spelling. After using this tool/service, the authors reviewed and edited the content as needed and take full responsibility for the content of the publication.

References:

[1] Attix, F.H. *"Introduction to Radiological Physics and Radiation Dosimetry"*. John Wiley & Sons, 2008.

[2] Sabbah, D.A.; Al-Basheer, A.; Abu Al-Rub, T.; Aljbour, S.; Al-Zoubi, H.; Alkarablieh, K.; Alsharif, M.; Khamis, S. "Structure-Based Design: Synthesis, X-ray Crystallography, and Biological Evaluation of N-Substituted-4-Hydroxy-2-Quinoline-3-Carboxamides as Potential Cytotoxic Agents." *Anti-Cancer Agents in Medicinal Chemistry*, 18, no. 2 (2018): 263-276. DOI: 10.2174/1871520617666170911171152.

[3] Dance, D.R. *"Diagnostic Radiology Physics: A Handbook for Teachers and Students"*. 2014.

[4] Barber, H.; Kahn, B.; Ahamad, A.; Kramar, S.; Yang, F.; Spence, M. "Semiconductor Pixel Detectors for Gamma-Ray Imaging in Nuclear Medicine." *Nuclear Instruments and Methods in Physics Research Section A: Accelerators, Spectrometers, Detectors and Associated Equipment*, 395, no. 3 (1997): 421-428. https://doi.org/10.1016/S0168-9002(97)00615-3.

[5] Kasap, S.; Pomerantz, H.; Kuhl, J.; Lee, D. "Amorphous and Polycrystalline Photoconductors for Direct Conversion Flat Panel X-ray Image Sensors." *Sensors*, 11 (2011): 5112-5157. https://doi.org/10.3390/s110505112.

[6] Parker, S.I.; Kenney, C.J.; Segal, J. "3D—A Proposed New Architecture for Solid-State Radiation Detectors." *Nuclear Instruments and Methods in Physics Research Section A: Accelerators, Spectrometers, Detectors and Associated Equipment*, 395, no. 3 (1997): 328-343. https://doi.org/10.1016/S0168-9002(97)00694-3.

[7] Luke, P.; Rossington, C.; Wesela, M. "Low Energy X-ray Response of Ge Detectors with Amorphous Ge Entrance Contacts." *IEEE Transactions on Nuclear Science*, 41, no. 4 (1994): 1074-1079. DOI: 10.1109/23.322861.

[8] Szeles, C. "CdZnTe and CdTe Materials for X-Ray and Gamma Ray Radiation Detector Applications." *Physica Status Solidi (b)*, 241, no. 3 (2004): 783-790. https://doi.org/10.1002/pssb.200304296.

[9] Batiha, Iqbal M., Jamal Oudetallah, Adel Ouannas, Abeer A. Al-Nana, and Iqbal H. Jebril. "Tuning the fractional-order PID-controller for blood glucose level of diabetic patients." *Int. J. Advance Soft Compu. Appl.*, 13, no. 2 (2021): 1-10.

[10] Stoumpos, C.C.; Malliakas, C.D.; Kanatzidis, M.G. "Crystal Growth of the Perovskite Semiconductor CsPbBr3: A New Material for

High-Energy Radiation Detection." *Crystal Growth & Design*, 13, no. 7 (2013): 2722-2727. https://doi.org/10.1021/cg400645t.

[11] I. M. Batiha, S. A. Njadat, R. M. Batyha, A. Zraiqat, A. Dababneh, and S. Momani, "Design fractionalorder PID controllers for single-joint robot arm model," *Int. J. Advance Soft Compu. Appl*, vol. 14, pp. 97-114, 2022. DOI: 10.15849/IJASCA.220720.07.

[12] Algadri, N.A.; Al-Diabat, A.M.; Ahmed, N.M. "Zinc Sulfide Based Thin Film Photodetector Prepared by Spray Pyrolysis." *Instrumentation Science & Technology*, (2022): 1-18. https://doi.org/10.1080/10739149.2022.2108832.

[13] Woggon, U. *Optical Properties of Semiconductor Quantum Dots*. Vol. 136. Springer, 1997.

[14] Lin, Lin, Siyao Liu, Sirui Fu, Shuangmei Zhang, Hua Deng, and Qiang Fu. "Fabrication of highly stretchable conductors via morphological control of carbon nanotube network." *Small*, 9, no. 21 (2013): 3620-3629. https://doi.org/10.1002/smll.201202306.

[15] Canham, L. *Handbook of Porous Silicon*. Springer International Publishing, 2014.

[16] Lawrence, W.G.; Huang, X.; Rojas, R.; Hay, J.; Wright, D.; Kim, J. "Quantum Dot-Organic Polymer Composite Materials for Radiation Detection and Imaging." *IEEE Transactions on Nuclear Science*, 59, no. 1 (2012): 215-221. DOI: 10.1109/TNS.2011.2178861.

[17] Ali, A.M.A.; Al-Husseini, M.; Al-Hmoud, S.; El-Shahawy, M. "Multilayer ZnO/Pb/G Thin Film Based Extended Gate Field Effect Transistor for Low Dose Gamma Irradiation Detection." *Nuclear Instruments and Methods in Physics Research Section A: Accelerators, Spectrometers, Detectors and Associated Equipment*, 987 (2021): 164833. https://doi.org/10.1016/j.nima.2020.164833.

[18] El-Eskandarany, M.S. *Mechanical Alloying: Energy Storage, Protective Coatings, and Medical Applications*. William Andrew, 2020. https://doi.org/10.1016/C2018-0-01722-3.

[19] Saha, J.; Murthy, S.; Gupta, A.; Bhatt, A.; Narayan, V. "On the Voltage Transfer Characteristics (VTC) of Some Nanoscale Metal-Oxide-Semiconductor Field-Effect-Transistors (MOSFETs)." In *Physics of Semiconductor Devices*, 211-214. Springer, 2014. DOI: 10.1007/978-3-319-03002-9_52.

Contribution of Individual Authors to the Creation of a Scientific Article (Ghostwriting Policy)

Conceptualization, Ahmad M. AL-Diabat and Natheer A. Algadri.; methodology, Ahmad M. AL-Diabat and Tariq AlZoubi and Naser M. Ahmed.; software,
Abdulsalam Abuelsamen and Osama Abu noqta.; validation, Ahmad M. AL-Diabat and and Ghaseb N. Makhadmeh.; formal analysis, Amal Mohamed Ahmed Ali and ALMUTERY AML.;
investigation, Ahmad M. AL-Diabat and Natheer A. Algadri.; resources, Ahmad M. AL-Diabat and Tariq AlZoubi and Naser M. Ahmed.; data curation, Ahmad M. AL-Diabat and Tariq AlZoubi and Naser M. Ahmed.; writing—original
draft preparation, A.M.A.A. and A.A; writing—review and editing, N.M.A., K.H.I., N.A.A., A.M.A.-D.,
I.A.W. and K.H.I.; visualization, N.A.K.; supervision, N.M.A. and N.A.K.; project administration,
O.A.A., A.A. and K.H.I.; funding acquisition, K.H.I. and O.A.A.

Sources of Funding for Research Presented in a Scientific Article or Scientific Article Itself

No funding was received for conducting this study.

Conflict of Interest

The authors have no conflicts of interest to.